

# Non-ENSO interannual rainfall variability in central Chile during austral winter

Aldo Montecinos · Michael V. Kurgansky ·  
Cristian Muñoz · Ken Takahashi

Received: 17 December 2010 / Accepted: 28 April 2011  
© Springer-Verlag 2011

**Abstract** The first principal component (PC1) of seasonal rainfall anomalies in central Chile during winter (June–August) is used to analyze the circulation anomalies related to wet and dry conditions, when near-normal or neutral SST anomalies are observed in the equatorial Pacific, i.e., during non-ENSO conditions. Eight wet and eight dry winter seasons were defined as the upper and lower terciles of PC1 for 24 non-ENSO winters in the period 1958–2000. Unlike the single process attributed to ENSO, during non-ENSO winter seasons, there are several sources triggering or modifying the propagation of the stationary waves that impact the rainfall regime in central Chile. Unfortunately, the multiple processes that seem to be involved in the modulation of the interannual rainfall variability in central

Chile, as seen in this work, limit the predictability of rainfall during non-ENSO conditions.

## 1 Introduction

El Niño–Southern Oscillation (ENSO) is the main source of climate variability on interannual timescales in many places of the planet. In central Chile, its influence has been recognized by several authors (e.g., Pittock 1980; Aceituno 1988), since Walker and Bliss (1932) defined the Southern Oscillation with a set of variables that included rainfall and pressure in Santiago of Chile. The ENSO-related rainfall variability in central Chile exhibits strong seasonality (Montecinos et al. 2000), with a well statistically defined warm–wet/cold–dry relationship during austral winter and spring restricted to the regions 30°–35° S and to 35°–38° S, respectively.

Central Chile exhibits a remarkably rainy season during austral winter, mainly due to cold fronts associated with migratory low-pressure systems embedded in the midlatitude westerlies. These systems reach their northernmost position in winter due to the annual movement of the South Pacific subtropical anticyclone (SPSA). The ENSO-associated circulation anomalies that force austral winter rainfall variability in central Chile can be described as a meridional dipole oriented between the SPSA and the Amundsen–Bellingshausen Seas in the Southern Ocean. Weaker (stronger) SPSA, especially on its poleward side, is related to an anticyclonic (cyclonic) system in the Amundsen–Bellingshausen Seas during El Niño (La Niña) conditions in the Tropical Pacific (Rutllant and Fuenzalida 1991; Montecinos and Aceituno 2003). During austral winter, an enhanced blocking activity, i.e., long-lasting quasi-barotropic anticyclones, over the Amundsen–

---

A. Montecinos · M. V. Kurgansky · C. Muñoz  
Departamento de Geofísica, Universidad de Concepción,  
Concepción, Chile

K. Takahashi  
Instituto Geofísico del Perú,  
Lima, Perú

A. Montecinos (✉)  
Department of Geophysics,  
Faculty of Physical and Mathematical Sciences,  
University of Concepcion,  
Casilla-160 C,  
Concepcion, Chile  
e-mail: amonteci@dgeo.udec.cl

M. V. Kurgansky  
A.M. Obukhov Institute of Atmospheric Physics,  
Russian Academy of Sciences,  
Moscow, Russia

C. Muñoz  
Department of Geophysics, University of Chile,  
Santiago, Chile

Bellingshausen Seas contributes to northward migration of the baroclinic storm track in the eastern South Pacific, when El Niño develops in the Tropical Pacific. Dry conditions in central Chile are favored by long-lasting and semi-permanent intense ridges in subtropical latitudes and a southward migration of the midlatitude storm track in the eastern South Pacific, and they are relatively more frequent during La Niña events (Montecinos and Aceituno 2003).

In the Southern Hemisphere, the main modes of variability of the atmospheric circulation on interannual and longer timescales have been amply described in the literature (see Mo 2000 and references therein). The first mode is a zonally symmetric pattern in the sea level pressure field with opposite signs between the Antarctica and midlatitudes. This mode has been named the High-Latitude Mode (Kidson 1999) or Southern Annular Mode, or Antarctic Oscillation (AAO) (Thompson and Wallace 2000), and it is not related to ENSO. The second and third modes of variability consist of wave train patterns called the Pacific South American (PSA) patterns: PSA1 and PSA2, respectively. They are in quadrature and depict a sequence of large-scale cyclones and anticyclones extending from the tropical Pacific into the Southern Ocean and eastern South America. The PSA1 has been related to ENSO forcing with the Rossby wave train source region located near the dateline in the Tropical Pacific. The PSA2 seems to be also generated in the Tropical Pacific, near eastern Australia, and related to a quasi-biennial component of ENSO (Mo 2000). In particular, the anticyclonic (cyclonic) system in the Amundsen–Bellingshausen Seas associated with wet (dry) conditions in central Chile is part of the PSA1 pattern generated by El Niño (La Niña) conditions in the central tropical Pacific (Rutllant and Fuenzalida 1991; Montecinos and Aceituno 2003).

The main extratropical source of interannual-to-interdecadal rainfall variability in the Southern Hemisphere is the AAO. The AAO forces rainfall fluctuations in southeastern South America during austral winter and late spring (Silvestri and Vera 2003), western South Africa during austral winter and spring (Reason and Rouault 2005), southeastern and southwestern Australia and western Tasmania (Hendon et al. 2007), northern Australia (Meneghini et al. 2007), and New Zealand (Renwick and Thompson 2006). On interannual timescales, an anti-correlation between an AAO index (linearly detrended) and rainfall in southern-central Chile is found, with the maximum effect at 40°S (Gillett et al. 2006). Thus, during the positive (negative) phase of the AAO, there is a reduction (increase) of rainfall. This relationship can be explained by the reduction in the midlatitude zonal flow and the associated frontal activity during the AAO (Garreaud et al. 2008). On the other hand, Quintana (2004) showed that AAO partially explains the observed negative long-

term trend of annual precipitation in the southern portion of central Chile (37°–43°S).

Several authors have demonstrated the influence of the recently discovered Indian Ocean Dipole (IOD) on the rainfall variability in many regions of the planet (e.g., Saji et al. 1999). The positive phase of the IOD mode is characterized by positive (negative) sea surface temperature (SST) anomalies in the western (southeastern) tropical Indian Ocean. The IOD mode has been related to rainfall interannual fluctuations in the Indonesian region (Saji et al. 1999), Indian summer Monsoon region (Terry et al. 2003), Australia (Ashok et al. 2003), Zimbabwe-East Africa (e.g., Conway et al. 2007; Manatsa et al. 2008), among other remote regions over Europe, northeast Asia, North and South America and South Africa (Saji and Yamagata 2003). In particular, Chan et al. (2008) found that SST forces a Rossby wave train from subtropical south Indian Ocean to the subtropical South Atlantic, reinforcing the South Atlantic subtropical anticyclone. According to Chan et al. (2008), this anomalous anticyclone drives anomalous divergence (convergence) of moisture over central Brazil (subtropical La Plata Basin).

The influence of extratropical SST anomalies on rainfall has been studied by several authors. For instance, Reason et al. (2002) showed that austral winter rainfall variability in the southwestern South Africa (SWSA) can be modulated by SST anomalies in the midlatitude South Atlantic and also by sea-ice extent in the Southern Ocean. These SST anomalies favor an increased (decreased) upstream cyclogenesis, a more northward (southward) position of midlatitude cold fronts, and an enhancement (decrease) of rainfall over SWSA. Ting et al. (1996) demonstrated the modulating impact of SST anomalies in the North Pacific on winter rainfall anomalies over the USA, which they related to midlatitude zonal mean flow variability. In this regard, Wang and Ting (2000) showed that about 45% of the winter rainfall variations are related to the Pacific SST anomalies, among which 35% are related to the North Pacific SST and associated extratropical atmospheric circulation anomalies and 10% are related to the tropical Pacific SST.

On the other hand, several authors have recently pointed out that there are two types of El Niño events, which are characterized by different SST anomaly patterns in the equatorial Pacific and different driving mechanisms (e.g., Ashok et al. 2007; Kao and Yu 2009). The canonical El Niño develops in the eastern equatorial Pacific, whereas during the new type of El Niño, the positive SST anomalies are located in the central equatorial Pacific. Larkin and Harrison (2005) presented evidence that these two distinct El Niño events lead to different temperature and rainfall anomalies during boreal fall and winter around the globe. Similarly, Weng et al. (2007) found changes in the

teleconnection patterns in the Pacific Ocean and their associated rainfall anomalies during austral winter.

The aim of the present paper is to describe the extratropical atmospheric circulation patterns associated with wet and dry austral winter seasons (hereafter just winter seasons) in central Chile that are not explained by teleconnection patterns generated in the tropical Pacific, i.e., occurring during non-ENSO winter seasons. The paper is organized as follows: Section 2 describes the used data and methodology. The obtained results are presented in Section 3. Finally, the results are discussed and concluding remarks are given in Section 4.

## 2 Data and methodology

The analysis is focused on the rainy season in central Chile, i.e., during the winter months from June to August, in the period 1958–2000. We used monthly rainfall time series from 63 stations in central Chile (30°–42°S). Large-scale atmospheric circulation anomalies are analyzed by using monthly National Center for Environmental Prediction/National Center for Atmospheric Research (NCEP-NCAR) reanalysis (NNR) (Kalnay et al. 1996): 500-hPa geopotential height (H500), sea level pressure (SLP), 300-hPa zonal wind component (U300), 1,000–200 hPa thickness (Z), precipitation rate, and the 200-hPa streamfunction. Also, the monthly values of the extended reconstructed global SST version 3 (Smith et al. 2008) and gridded surface air temperature and precipitation over South America produced by the University of Delaware (UD) (Legates and Willmont 1990a, b) are used. The linear trend was removed from all time series.

The standardization of rainfall data in central Chile consisted in the transformation of each time series into their percentiles, using the cumulative probability estimator  $p(x_i) = i/(n+1)$  (Wilks 2006), where  $i$  represents the position in time (rank) of an individual rainfall series ( $x_i$ ), after the  $n$  values (43) are sorted from lower to higher values. Thus, all standardized rainfall anomalies vary from  $-0.48$  to  $0.48$ , with a standard deviation of  $0.28$ . The Empirical Orthogonal Function (EOF) is used to describe the spatial and temporal covariability of the fields. To determine the significance of the EOF modes, the sampling error criteria of North et al. (1982) is used. In other analyses, the statistical significance is evaluated by Monte Carlo tests at 95% of confidence level (von Storch and Zwiers 1999).

The non-ENSO rainfall variability and its associated large-scale circulation anomalies are found by focusing on winter seasons characterized by neutral SST conditions in the tropical Pacific. The SST anomaly in the region Niño 3.4 is widely used in ENSO related studies, i.e., in the

identification of El Niño and La Niña events. However, it has been proven that Niño 3.4 SST anomalies cannot distinguish between the two types of El Niño (Trenberth and Stepaniak 2001; Kao and Yu 2009). For that reason, the non-ENSO winters are defined as those ones when none of the SST Niño's indices in the equatorial central Pacific had standardized SST anomalies exceeding in magnitude one standard deviation (Fig. 1). According to this procedure, 24 non-ENSO events were found during the winter season in the period 1958–2000.

Following Vera et al. (2004), the source of stationary wave activity is diagnosed by computing the horizontal components of the wave activity flux vector as defined by Plumb (1985); see Schubert and Park (1991) for the definition of the horizontal flux components based on the eddy component of the 200-hPa streamfunction. According to Karoly et al. (1989), the horizontal stationary wave activity flux is a useful method to diagnose the horizontal propagation of quasi-stationary waves. As in Karoly et al. (1989), the wave activity flux is calculated from the zonally asymmetric part of the 200-hPa streamfunction anomalies. Regions with divergent flux vectors denote the export of wave activity. This diagnostic procedure is able to identify the Rossby waves generated by a tropical heating source, to identify the source region and to make evident propagation of stationary wave activity (Vera et al. 2004, and reference therein).

Finally, the main—after ENSO—large-scale climate variability modes, i.e., the AAO and IOD are used. The AAO index is defined as the first principal component of the 850-hPa geopotential height anomalies south of 20°S (Thompson and Wallace 2000; <http://jisao.washington.edu/data/aa/>). Also, the IOD index was calculated as the difference between the SST anomalies in the tropical western Indian Ocean (50°–70° E, 10° S–10° N) and the tropical southeastern Indian Ocean (90°–110° E, 10° S–0° S),

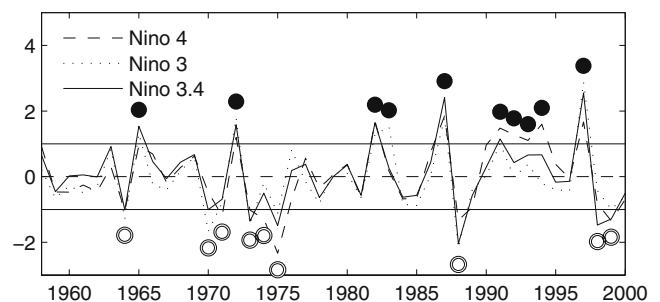


**Fig. 1** Time series of the winter (June–August) SST anomalies (SSTA) in the region Niño 4 (5° S–5° N, 160° E–150° W), Niño 3 (5° S–5° N, 150°–90° W), and Niño 3.4 (5° S–5° N, 170°–120° W) in the period 1958–2000. The time series were standardized. Black (open) circles show winter seasons with SSTA equal or higher (lower) than 1 (–1) standard deviation in any of the three Niño's SSTA indices

following Saji et al. (1999). In both cases, the linear trend was removed.

### 3 Results

#### 3.1 Rainfall index

The first EOF mode of the 63 standardized rainfall anomalies in central Chile, using the 24 non-ENSO winter seasons, accounts for 91% of the total variance, while the second EOF mode explains 4%. According to the criteria of North et al. (1982), the first and second EOF modes are well separated from the subsequent modes. Figure 2 shows the first EOF pattern. Most of the variance of the main EOF mode is concentrated between 33° and 36° S, although correlations larger than 0.7 between the first principal component and individual standardized rainfall anomalies span from 30.5° to 39.5° S. The second EOF pattern (not shown) exhibits a meridional dipole with the largest values in the northern part of central Chile (30°–31° S).

Figure 3 depicts the scatter diagram of the first and second principal components (PC1 and PC2, respectively). Vertical segmented lines show the lower and upper tercile limits based on the cumulative probability distribution of the PC1. Thus, eight wet (1961, 1963, 1966, 1977, 1978,

**Fig. 2** First EOF pattern of rainfall in central Chile (30°–42°S), using 63 standardized rainfall anomalies during 24 non-ENSO winters (June–August) in the period 1958–2000. The EOF is shown as correlation between the first principal component and the individual time series. Correlations are shaded every 0.1 for magnitudes of at least 0.5. Solid (segmented) lines indicate positive (negative) correlations

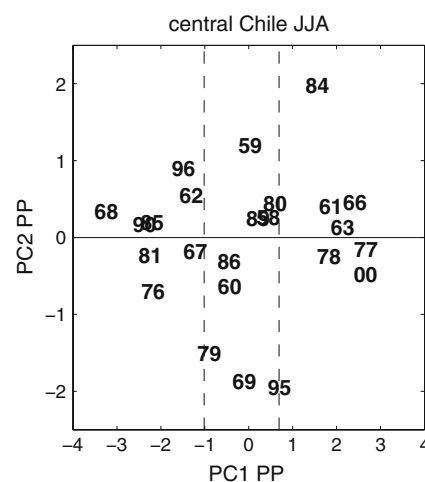
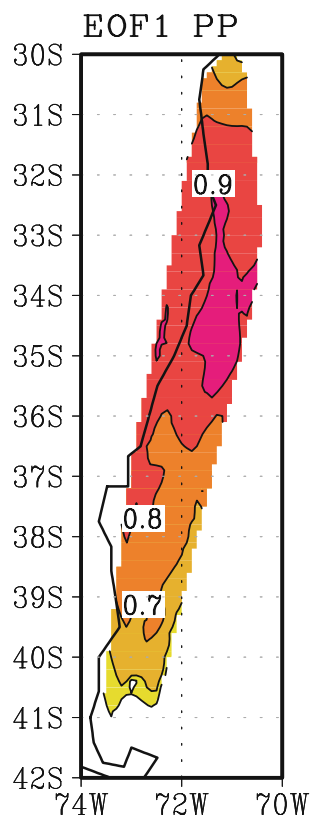


**Fig. 3** Scatter diagram between the first and second principal components (PC1 and PC2) of rainfall in central Chile (30°–42° S), using 63 standardized rainfall anomalies during 24 non-ENSO winters (June–August) in the period 1958–2000. Vertical segmented lines indicate the upper and lower limit of terciles, defining wet and dry winter seasons in central Chile during non-ENSO conditions

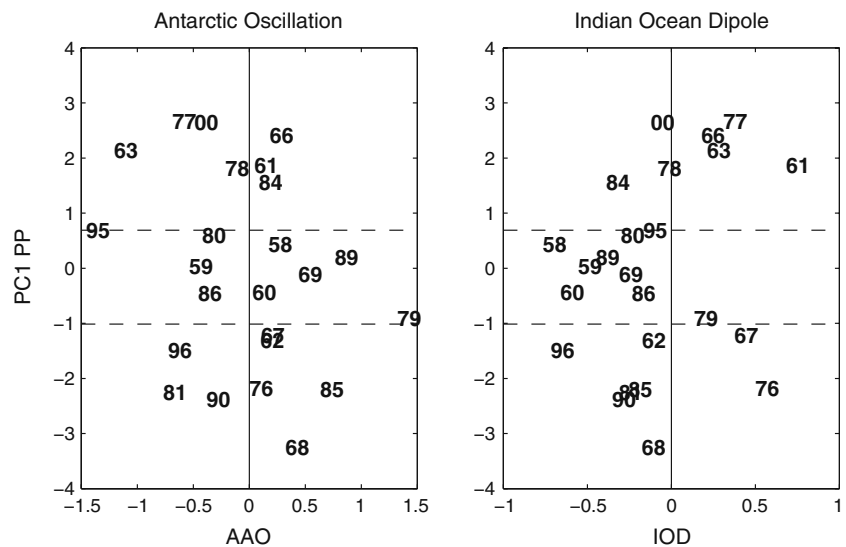
1984, 1995, and 2000) and eight dry (1962, 1967, 1968, 1976, 1981, 1985, 1990, and 1996) conditions are defined as the upper and lower terciles. The most clear meridional dipole for wet conditions occurs during 1984 and 1995, but with opposite PC2 sign. While in the winter of 1984, the wet (dry to normal) conditions were confined to the north (south) of 36° S; in 1995, the wet (dry to normal) conditions were observed to the south (north) of 35° S (not shown). When this analysis is performed using the 43 non-ENSO and ENSO seasons, both the EOF patterns and the PCs are very close to those described previously.

A straightforward analysis of the rainfall anomalies in central Chile during non-ENSO conditions is the direct comparison with the large-scale climate modes: AAO and IOD. This comparison is shown in Fig. 4 as scatter diagrams of PC1 and both climate modes during the 24 non-ENSO winters. The correlations between PC1 and AAO, and IOD are near zero (−0.21 and 0.12, respectively). There exists a slight tendency to have dry (wet) conditions during the negative (positive) phase of IOD. The same occurs with AAO. Five of eight dry (wet) winters appear during the positive (negative) phase of AAO. These results suggest a rather complicated non-linear functional relationship, in which AAO and IOD would play, at most, a secondary role.

#### 3.2 Circulation anomalies for individual wet and dry winters

In principle, a single process responsible for wet and dry winters during non-ENSO conditions is not expected.

**Fig. 4** Scatter diagram between the first principal component (PC1) of the standardized rainfall in winter characterized by neutral SST conditions in the tropical Pacific, and the **a** Antarctic Oscillation (AAO) index and the **b** Indian Ocean Dipole (IOD) index (see text for details). *Horizontal segmented lines* indicate the upper and lower limit of terciles, defining wet and dry winter seasons in central Chile during non-ENSO conditions



Figures 5 and 6 show the standardized H500 and U300 anomalies during each of the eight wet and eight dry winter seasons, respectively. Both U300 and H500 are commonly used in climate variability studies.

In Fig. 5, positive standardized U300 anomalies are located over central Chile during most of wet winter seasons, with a tendency of founding negative U300 to the south during 1963, 1977, 1984, and 1995. This pattern is not clear in year 2000, during which positive U300 appear in northern Chile, and is completely reversed in 1978, when negative U300 are located over central Chile.

For wet conditions in central Chile, the standardized H500 anomalies show a variety of patterns (Fig. 5) that are not simple to classify. Positive U300 over central Chile are part of a negative H500 pattern (cyclonic circulation anomaly) centered to the south (1977, 1984, and 1995). In 1963, negative H500 anomalies are located in the eastern South Pacific with a northwest–southeast orientation. These cyclonic anomalies at 500 hPa have their manifestation at the surface. In fact, standardized SLP anomalies also present negative values during these wet winters (not shown). In 1966, a negative H500 pattern is found over central Chile, but it seems to be too weak to have a clear cyclonic circulation anomaly. In this case, negative SLP anomalies are also located over central Chile.

In the wet winter of 1977, there is a cyclonic anomaly pattern over the tip of South America (Fig. 5). Unlike 1995, with the strongest cyclone in the same region, in 1977 the anticyclonic counterpart in the Southern Ocean is located over the Weddell Sea. It is remarkable that the positive H500 pattern, centered at about 35°S–100°W, is also present at the surface as strong positive SLP anomalies (not shown). In the polar flank of this anticyclone, positive U300 appear off central Chile. This pattern, which is characterized by positive–negative–positive H500 and SLP

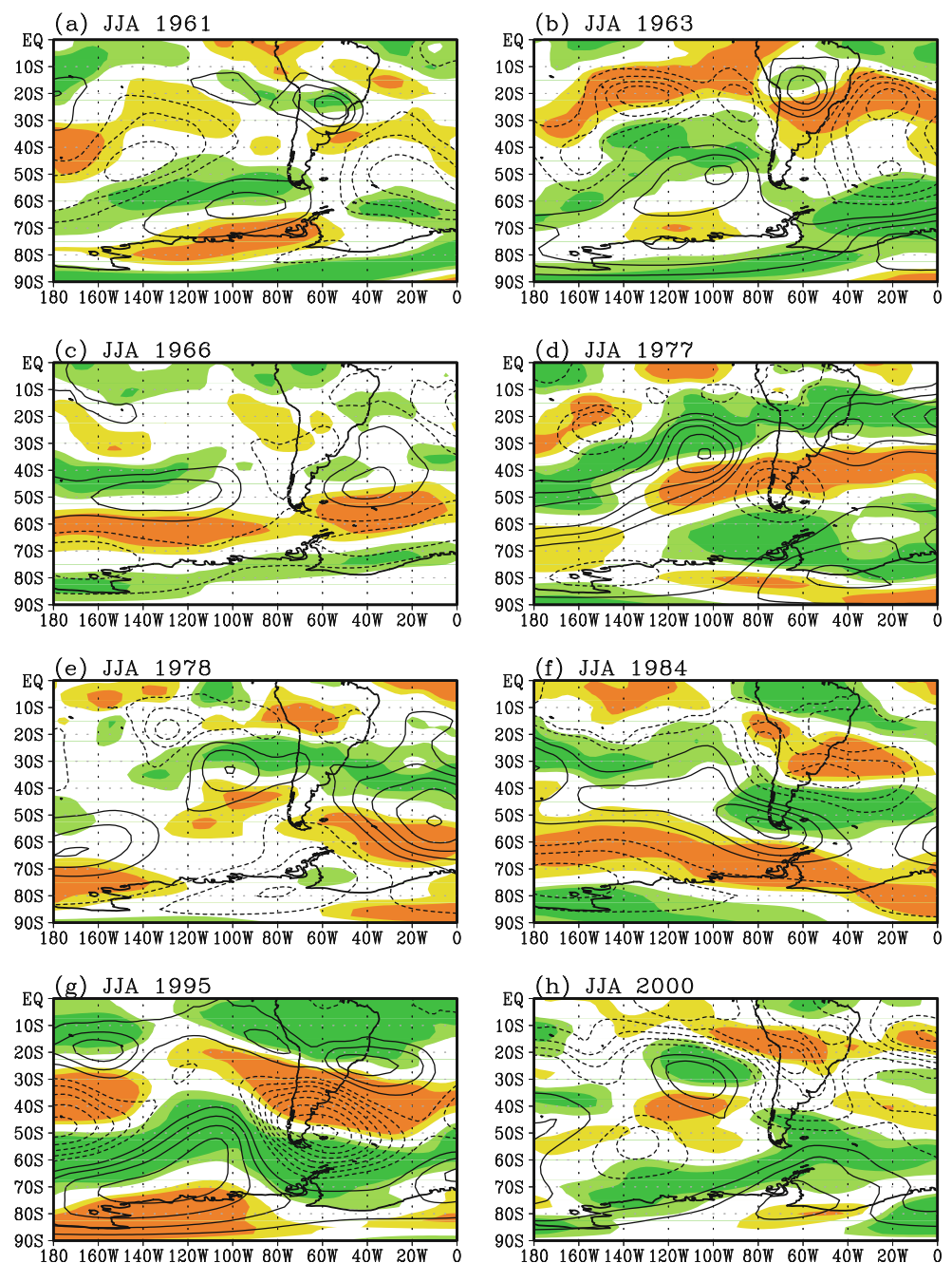
anomalies oriented from the eastern South Pacific to the Weddell Sea is very similar to that observed in 2000. In 1978, the anticyclone is also present along 35° S in the eastern South Pacific, but with negative SLP anomalies (not shown).

During the dry winter seasons (Fig. 6), negative U300 anomalies appear over central Chile with positive standardized anomalies located to the south during 1962, 1968, 1981, 1985, 1990, and 1996. In all these winter seasons, the described upper circulation pattern is accompanied by positive H500 values, defining a well-structured anticyclonic anomaly with positive standardized SLP anomalies at the surface (not shown). The described pattern is not observed in 1976, being the opposite during 1967, i.e., with positive U300 and negative H500 anomalies when dry conditions are present in central Chile.

In general, the anticyclonic anomaly is located at about 45°–50° S over Patagonia, although in 1968, it is clearly shifted to the southwestern South Atlantic, while in 1981 it is located off southern Chile (Fig. 6). In 1990, the anticyclonic anomaly is located at about 35° S off central Chile that resembles the pattern for the wet austral winter seasons of 1977, 1978, and 2000 (Fig. 5). Unlike these wet season-related patterns, the anticyclonic anomaly in 1990 is located close to the continent with its center at about 80° W, driving negative U300 anomalies over central Chile.

Similar to 1976, in 1967, there is no correspondence between the upper and surface circulation anomalies over central Chile. While the upper circulation shows negative H500 anomalies (Fig. 6), the SLP pattern exhibits positive anomalies (not shown). It is worth noting that an SPSA index, computed as the spatial average of SLP in the region 35°–20° S and 110°–80° W, shows its largest positive anomaly during 1967 compared with all non-ENSO austral winter seasons (not shown).

**Fig. 5** The 500-hPa geopotential height (H500) and 300-hPa zonal wind (U300) standardized anomaly fields, for each wet winter (June–August) in central Chile, during neutral SST conditions in the equatorial Pacific: **a** 1961, **b** 1963, **c** 1966, **d** 1977, **e** 1978, **f** 1984, **g** 1995, and **h** 2000. Positive (negative) H500 standardized anomalies are contoured with *solid* (*segmented*) lines, every 0.5 standard deviation. Positive (negative) U300 standardized anomalies are shaded with *warm* (*cold*) colors, using the interval  $-1.0$ ,  $-0.5$ ,  $0.5$ , and  $1.0$  of standard deviation. The zero line is omitted

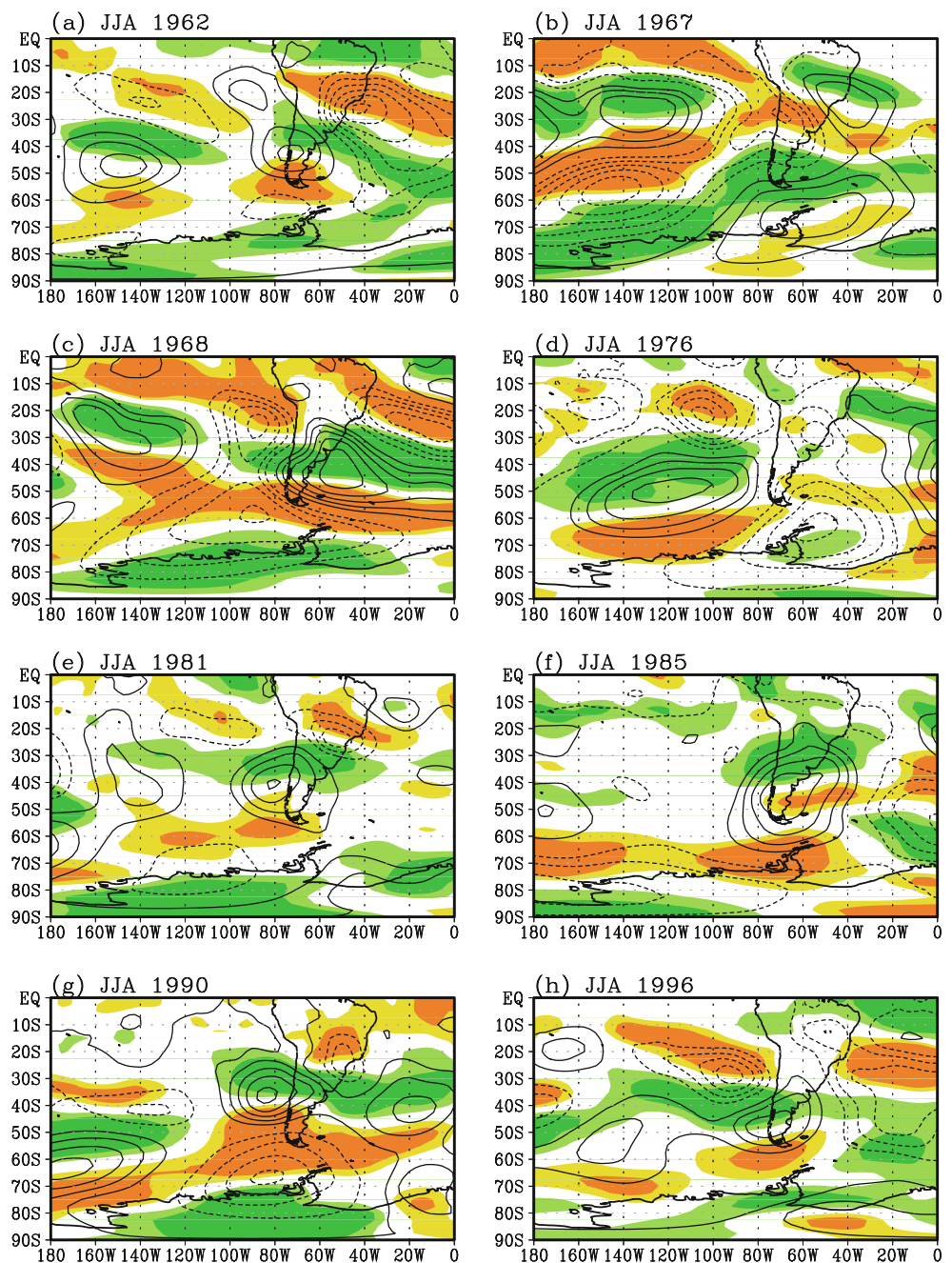


### 3.3 Regional circulation pattern

A closer examination of the seasonal U300 and H500 variance during ENSO and non-ENSO winter seasons, reveals an important distinction between the related extratropical circulation anomalies. Figure 7a shows the difference between the U300 standard deviation fields calculated for 24 non-ENSO and 19 ENSO winter seasons, respectively. The same is shown in Fig. 7b but for H500. The statistical significance at 5% level is also shown as shaded areas and is achieved by Monte Carlo experiments. These consisted in constructing a large number of independent

realizations of the standard deviation differences. The following steps were performed 1,000 times: (1) resampling of 19 and 24 winter seasons falling into the period 1958 – 2000; (2) calculation of the standard deviation field for each set of 19 and 24 winters; (3) calculation of the difference between them. For each grid point, there is a series of 1,000 differences of standard deviations obtained by a random process. From this random distribution, the percentiles 2.5% and 97.5% are determined. If the observed difference is outside the random interval defined by the percentiles, the value is significant at 5% level and the grid is shaded in Fig. 7.

**Fig. 6** As in Fig. 5, but for dry winter seasons: **a** 1962, **b** 1967, **c** 1968, **d** 1976, **e** 1981, **f** 1985, **g** 1990, and **h** 1995



The most remarkable difference between the non-ENSO variance and the ENSO variance in extratropical South America is located over Patagonia (Fig. 7b). During non-ENSO winters, the variance of seasonal H500 is almost twice that of ENSO winters (not shown). Although there is an increase of the U300 variance over central Chile, this signal is not significant.

The EOF analysis is applied to the combined standardized U300–H500 anomalies in the regions 60°–30° S and 90°–50° W, using the 43 winter seasons in the period 1958–2000. The first EOF (EOF1) accounts for 37% of the total variance and is well separated of the subsequent modes,

according to the error sampling criteria of North et al. (1982). The positive (negative) EOF1 phase corresponds to an anticyclonic (cyclonic) anomaly over Patagonia with upper easterly (westerly) anomalies along 30°–35° S (Fig. 8). The scatter diagram of the PC1 of rainfall in central Chile, using the period 1958–2000, and the PC1 of the combined U300–H500 (PC1 U300–H500) is shown in Fig. 9. The correlation between both time series is  $-0.59$ . However, since most of the ENSO winters present similar slightly negative values of the PC1 U300–H500, except for La Niña winter of 1998, the variability is almost exclusively related to non-ENSO rainfall winters. In consequence, the

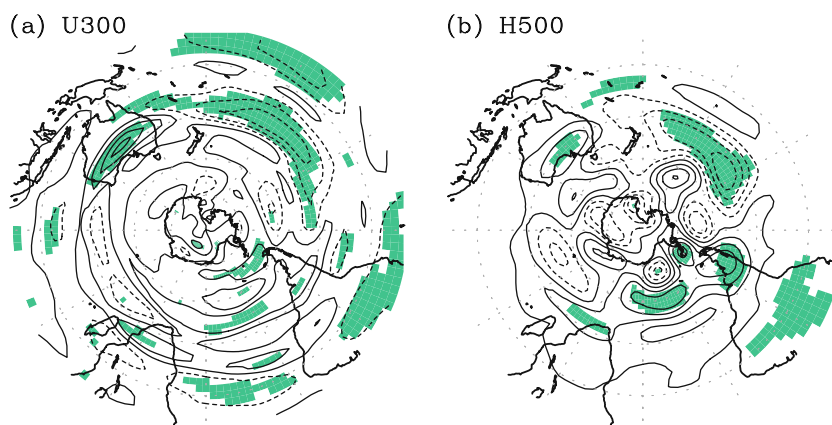


**Fig. 7** Difference between the standard deviation of 24 non-ENOS and the standard deviation of 19 ENOS winter seasons of (a) 300-hPa zonal wind (U300) anomalies and (b) 500-hPa geopotential height (H500) anomalies. Standard deviations differences are contoured

every  $0.5 \text{ ms}^{-1}$  for U300 and 20 m for H500. Solid (segmented) lines indicate positive (negative) values. Shaded areas are significant at 95% of confidence, according to a Monte Carlo test (see text for details)

anticyclonic (cyclonic) anomaly over Patagonia and the associated upper level easterly (westerly) wind anomalies along  $30^{\circ}$ – $35^{\circ}$  S are most related to dry (wet) rainfall condition in central Chile. Comparatively, the dry non-ENSO winters show a stronger signal in PC1 U300–H500 than the wet non-ENSO winters, showing higher positive values of the PC1 U300–H500 in relation to the negative PC1 of rainfall.

Despite the above, the analysis of individual circulation fields based on Figs. 5 and 6 shows that there is no single circulation pattern associated with the dry and wet non-ENOS conditions in central Chile. Although there is a clear tendency for finding positive H500 anomalies over Patagonia and negative U300 over central Chile when dry

conditions are observed, as indicated in the previous section, the position of the anticyclone system is different from case to case, with the anticyclonic anomaly centered over Patagonia in 1985, oriented to the southeastern Pacific in 1981, and oriented to the southwestern Atlantic in 1968 (Fig. 6).

Figure 10 shows the standardized SST, 1,000–200 hPa thickness (Z), and surface air temperature anomalies, and the wave activity flux vectors computed from the 200-hPa streamfunction anomalies for four selected cases, corresponding to extreme values of PC1 U300–H500 during dry and wet non-ENSO winters: three dry (1968, 1985, and 1990) and one wet (1995) winter seasons (Fig. 9). First of all, the anticyclone located near Patagonia during the dry winters is characterized by positive Z anomalies and positive air temperature at the surface of

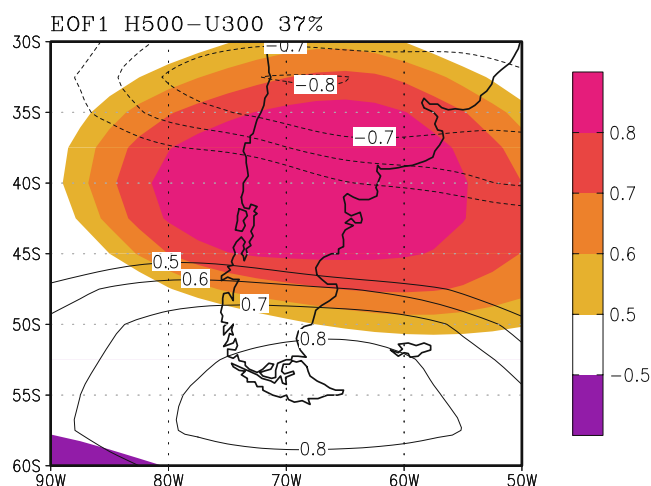


**Fig. 8** First EOF pattern of the combined 500-hPa geopotential height (H500)—300-hPa zonal wind (U300) standardized anomalies in the region  $60^{\circ}$ – $30^{\circ}$  S,  $90^{\circ}$ – $50^{\circ}$  W, using 43 winter seasons in the period 1958–2000. Correlations are shaded (contoured) every 0.1 when the absolute values are of at least 0.5 for H500 (U300). Zero line is omitted

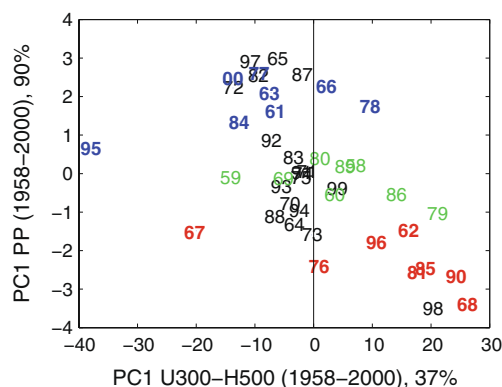
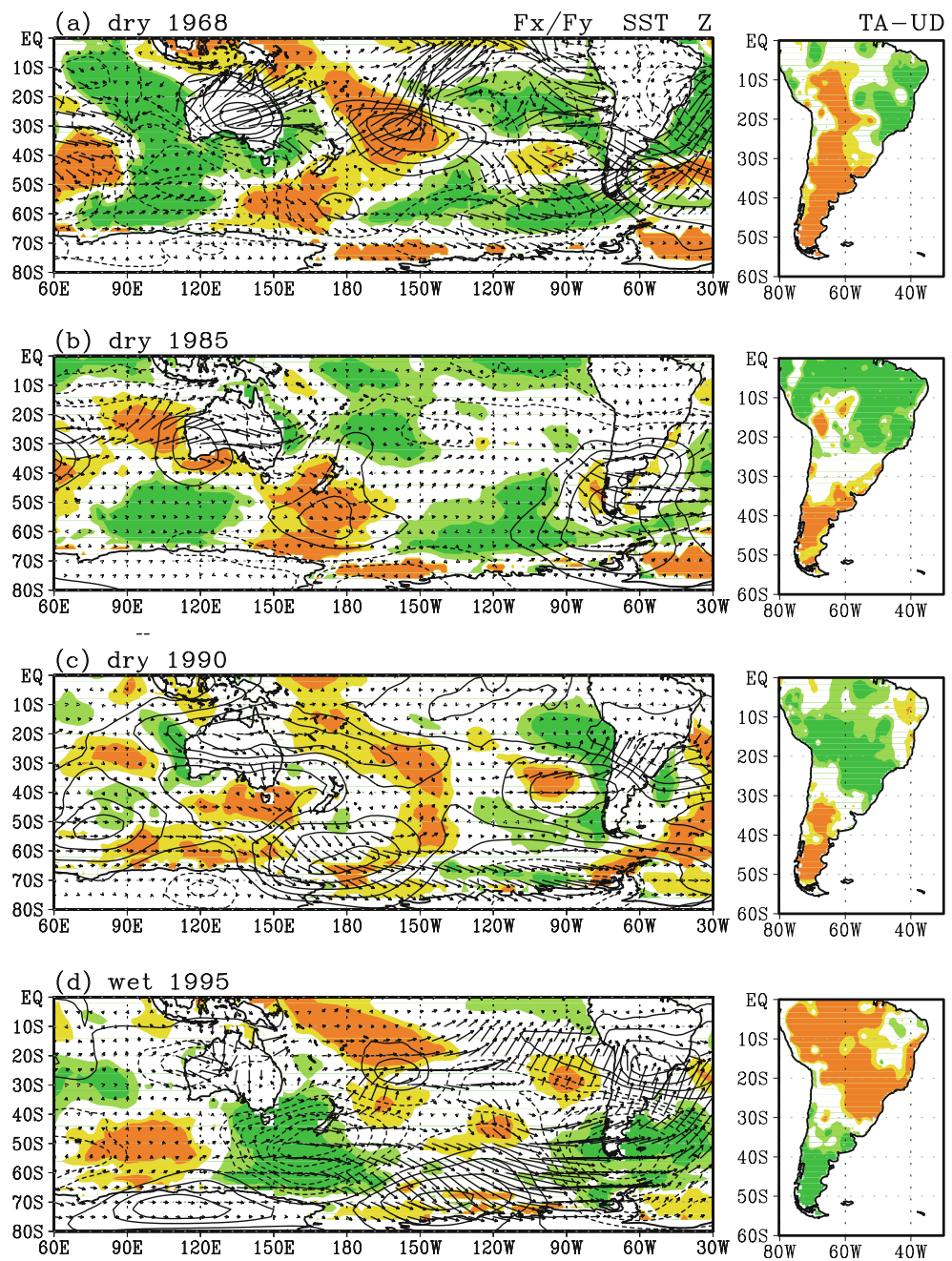


**Fig. 9** Scatter diagram between the first principal component (PC1) of the combined 500-hPa geopotential height (H500)—300-hPa zonal wind (U300) standardized anomalies in the region  $60^{\circ}$ – $30^{\circ}$  S,  $90^{\circ}$ – $50^{\circ}$  W, and the PC1 of 63 standardized rainfall anomalies in central Chile, using 43 winter seasons in the period 1958–2000. Red, green, and blue numbers correspond to wet, normal, and dry winter seasons during non-ENSO conditions, respectively

**Fig. 10** Horizontal wave activity fluxes (*vectors*), standardized SST (*shading*), and 1,000–200 hPa thickness (*Z*) (*contour*) anomalies [*left panels*], and the standardized air surface temperature anomalies (*shading*) [*right panels*], during the dry winters of **a** 1968, **b** 1985, and **c** 1990, and during the wet winter of **d** 1995. The *Z* anomalies are contoured every 0.5 standard deviation, with *solid (segmented) lines* indicating positive (negative) values. Positive (negative) standardized SST and surface air temperature anomalies are shaded with *warm (cold) colors*, using the interval  $-1.0, -0.5, 0.5,$  and  $1.0$  of standard deviation



the extratropical South America. The opposite is also evident for the wet winter of 1995. The thermal structure of the circulation system over Patagonia is a common feature for almost all wet and dry winter seasons (not shown). The horizontal wave activity fluxes suggest a variety of sources of the stationary waves over the South Pacific and Southern Ocean. A clear wave train is seen during 1995, starting from the Southern Ocean, south of Australia, into South America. In the winter of 1990, the anticyclone located off central Chile seems to be part of an anticyclone–cyclone pair originated along 30° S at about 120° W. Similarly, in 1985, the source seems to be located

off central Chile in the subtropics at about 90° W. Finally, in the dry winter of 1968, the anticyclone located over Patagonia but centered in the southwestern Atlantic Ocean seems to be a part of two wave trains, one originated along 50° S at about 150° E and the other moving from the subtropics at about 120° W.

#### 4 Discussion and concluding remarks

The first principal component (PC1) of rainfall anomalies in central Chile during winter (June–August) is used to

analyze the circulation anomalies related to wet and dry conditions, when near-normal or neutral SST anomalies are observed in the equatorial Pacific, i.e., during non-ENSO conditions. Eight wet and eight dry winter seasons were defined as the upper and lower terciles of PC1 for 24 non-ENSO winters in the period 1958–2000.

The individual circulation anomalies during wet and dry winter seasons (Figs. 5 and 6), as well as the EOF analysis of the combined H500–U300 standardized anomalies (Figs. 8 and 9), show that most wet and dry winter seasons are related to upper westerly and easterly wind anomalies over central Chile, respectively. Garreaud (2007) found a significant and positive correlation between rainfall and U300 based on monthly anomalies, particularly over midlatitudes in the South Pacific and along the western side of the Andes. He argued that orographic effects superimposed to the frontal activity increased the correlation locally. When seasonal and annual means were used for the correlation analysis, Garreaud (2007) found similar patterns, but a weakening in the relationship. Here, the local correlation between PC1 and U300 is in average at about 0.52, which is significant albeit rather small. However, seven (six) out of eight wet (dry) non-ENSO winter seasons occur in the presence of upper level westerlies (easterlies) over central Chile.

The larger variance in seasonal H500 during non-ENSO winters indicates a stronger variability over Patagonia, indicating that the mechanism involving cyclonic and anticyclonic anomalies is not as active during ENSO winters. To this respect, the EOF1 of the combined U300–H500 standardized anomalies and its association with the PC1 of the rainfall anomalies in the period 1958–2000, suggest that there is a statistically significant linear relationship between them. However, the scatter diagram in Fig. 9 suggests that dry winter seasons are closely related to anticyclonic conditions over Patagonia with the subsequent zonal flow blocking over central Chile. The analysis of individual circulation anomalies shows that the anticyclone systems can be centered over Patagonia or can be elongated eastward into the Atlantic Ocean or to the west in the South Pacific, but the upper level easterlies over central Chile are similar.

Berbery and Núñez (1989) studied a blocking episode occurred in the period June 2–9, 1985. During this period, precipitation was not registered in stations located between 30° S and 38° S in central Chile, and 1985 is one of the dry winter seasons during non-ENSO conditions selected in this work. Based on numerical simulations performed with a hemispheric shallow-water model, Berbery and Núñez (1989) supported the mechanisms proposed by Charney and DeVore (1979) and Kalnay-Rivas and Merkiné (1981), in which the persistence and stationary position of the

blocking anticyclone can occur as a result of resonance enhancement of Rossby lee waves. The idea is that a source of transient Rossby waves upstream of the large-scale orography interact with the forced stationary Rossby waves excited by orography, by generating an anticyclone–cyclone pair-oriented southwest–northeast. According to Kalnay-Rivas and Merkiné (1981), this pattern resembles an omega-type blocking pattern (see their Fig. 4.11), where the blocking system is located southeast of the mountain. To simulate the blocking system located over Patagonia in June 1985 (see Fig. 1 in Berbery and Núñez 1989), the upstream transient source of Rossby waves was located at 35° S–135° W. The transient source of Rossby waves in the eastern Pacific Ocean at midlatitudes can be related to SST anomalies and enhanced baroclinicity with regular cyclogenesis (Kalnay-Rivas and Merkiné 1981; Berbery and Núñez 1989; Schubert and Park 1991). In order to obtain a more comprehensive picture on the origin of the systems forcing interannual rainfall variability in central Chile, numerical experiments are needed.

As a reference, the number of days with precipitation in Concepción (~37° S) in central Chile during the winter months (June to August) is 45. This climatological number decreases (increases) to the north (south) in central Chile. In average, there are 52 days with rainfall during the eight wet winter seasons in comparison to 38 days during the eight dry winter seasons. The difference between wet and dry conditions during the rainy seasons is at about 2 weeks. Thus, the occurrence of two or three blocking episodes can produce a quite large difference in the rainfall regime in central Chile.

To conclude, most of wet (dry) winter seasons during non-ENSO conditions are related to upper westerly (easterly) wind anomalies over central Chile. In most cases where a positive relation between U300 and rainfall anomalies exists, positive (negative) H500 anomalies over Patagonia are characterized by warm (cold) conditions from surface to the entire troposphere. For dry winter seasons, it is argued that the resonance between transient Rossby waves generated in the eastern South Pacific at midlatitudes, and stationary Rossby waves generated by Andes produces a blocking system located in southern South America. Unlike the single process attributed to ENSO, during non-ENSO winter seasons, there are several sources in the South Pacific and Southern Ocean triggering or modifying the propagation of the stationary waves that impact the rainfall regime in central Chile. Unfortunately, the multiple processes that seem to be involved in the modulation of the interannual rainfall variability in central Chile, as seen in this work, limit the predictability of rainfall during non-ENSO conditions. Considering these results, it is not surprising that the relationship between the PC1 and two leading climate modes related to interannual

rainfall variability in several places in the Southern Hemisphere, i.e., the AAO and IOD, is not significant.

**Acknowledgments** We wish to thank H. Graßl and an anonymous reviewer for their helpful comments on the original manuscript. This work was supported by Comisión Nacional de Investigación Científica y Tecnológica (CONICYT)-Chile through grant Fondecyt 1080058. NCEP–NCAR reanalysis data were provided by the Climate Diagnostic Center (NOAA). Rainfall data was supplied by the National Weather Service (DMC) and the Bureau of Water Management (DGA-MOP). Most figures were produced with the Grid Analysis and Display System (GrADS).

## References

- Aceituno P (1988) On the functioning of the Southern Oscillation in the South American sector. Part I: surface climate. *Mon Weather Rev* 116:505–524
- Ashok K, Guan Z, Yamagata T (2003) Influence of the Indian Ocean Dipole on the Australian winter rainfall. *Geophys Res Lett* 30:1821. doi:10.1029/2003GL017926
- Ashok K, Behera SK, Rao SA, Weng H, Yamagata T (2007) El Niño Modoki and its possible teleconnection. *J Geophys Res* 112: C11007. doi:10.1029/2006JC003798
- Berberly EH, Núñez MN (1989) An observational and numerical study of blocking episodes near South America. *J Clim* 2:1352–1361
- Chan SC, Behera SK, Yamagata T (2008) Indian ocean dipole influence on South American rainfall. *Geophys Res Lett* 35: L14S12, 10.1029/2008GL034204
- Charney JG, DeVore JG (1979) Multiple flow equilibria in the atmosphere and blocking. *J Atmos Sci* 36:1205–1216
- Conway D, Hanson CE, Doherty R, Persechino A (2007) GCM simulations of the Indian Ocean dipole influence on East African rainfall: present and future. *Geophys Res Lett* 34:L03705. doi:10.1029/2006GL027597
- Garreaud RD (2007) Precipitation and circulation covariability in the extratropics. *J Clim* 20:4789–4797
- Garreaud RD, Vuille M, Compagnucci R, Marengo J (2008) Present-day South American climate. *Palaeogeography, Palaeoclimatology, Palaeoecology* 281:180–195. doi:10.1016/j.paleo.2007.10.032
- Gillett NP, Kell TD, Jones PD (2006) Regional climate impacts of the Southern Annular Mode. *Geophys Res Lett* 33:L23704. doi:10.1029/2006GL027721
- Hendon HH, Thompson DWJ, Wheeler MC (2007) Australian rainfall and surface temperature variations associated with the Southern Hemisphere Annular Mode. *J Clim* 20:2452–2467
- Kalnay-Rivas E, Merkin LO (1981) A simple mechanism for locking. *J Atmos Sci* 38:2077–2091
- Kalnay E et al (1996) The NCEP/NCAR 40-year reanalysis project. *Bull Am Meteorol Soc* 77:437–471
- Kao H-Y, Yu J-Y (2009) Contrasting Eastern-Pacific and Central-Pacific types of ENSO. *J Clim* 22:615–632
- Karoly DJ, Plumb RA, Ting M (1989) Examples of the horizontal propagation of quasi-stationary waves. *J Atmos Sci* 46:2802–2811
- Kidson JW (1999) Principal modes of Southern Hemisphere low frequency variability obtained from NCEP–NCAR reanalysis. *J Clim* 12:2808–2830
- Larkin NK, Harrison DE (2005) On the definition of El Niño and associated seasonal average U.S. weather anomalies. *Geophys Res Lett* 32:L16705. doi:10.1029/2005GL022860
- Legates DR, Willmont C (1990a) Mean seasonal and spatial variability in gauge-corrected, global precipitation. *Int J Climatol* 10:111–127
- Legates DR, Willmont C (1990b) Mean seasonal and spatial variability in global surface air temperature. *Theor Appl Climatol* 41:11–21
- Manatsa D, Chingombe W, Matarira CH (2008) The impact of the positive Indian Ocean dipole on Zimbabwe droughts. *Int J Climatol* 28:2011–2029
- Meneghini B, Simmonds I, Smith IN (2007) Association between Australian rainfall and the southern annular mode. *Int J Climatol* 27:109–121. doi:10.1002/joc.1370
- Mo KC (2000) Relationships between low-frequency variability in the Southern Hemisphere and sea surface temperature anomalies. *J Clim* 13:3599–3620
- Montecinos A, Díaz A, Aceituno P (2000) Seasonal diagnostic and predictability of rainfall in subtropical South America based on tropical Pacific SST. *J Clim* 13:746–758
- Montecinos A, Aceituno P (2003) Seasonality of the ENSO-related rainfall variability in central Chile and associated circulation anomalies. *J Clim* 16:281–296
- North GR, Bell TL, Cahalan RF, Moeng FJ (1982) Sampling errors in the estimation of empirical orthogonal functions. *Mon Weather Rev* 110:699–706
- Pittock AB (1980) Patterns of climatic variation in Argentina and Chile. Part I: precipitation, 1931–1960. *Mon Weather Rev* 108:1347–1361
- Plumb RA (1985) On the three-dimensional propagation of stationary waves. *J Atmos Sci* 42:217–229
- Quintana J (2004) Factors involved in the interdecadal precipitation variability in Chile (in Spanish). M.S. thesis, Department of Geophysics, Universidad de Chile, 88 pp
- Reason CJC, Rouault M (2005) Links between the Antarctic Oscillation and winter rainfall over western South Africa. *Geophys Res Lett* 32:L07705. doi:10.1029/2005GL022419
- Reason CJC, Rouault M, Melice J-L, Jagadheesha D (2002) Interannual winter rainfall variability in SW South Africa and large scale ocean–atmosphere interactions. *Meteorol Atmos Phys* 80:19–29
- Renwick J, Thompson DWJ (2006) The southern annular mode and New Zealand climate. *Water Atmos* 14:24–25
- Rutllant J, Fuenzalida H (1991) Synoptic aspects of the central Chile rainfall variability associated with the Southern Oscillation. *Int J Climatol* 11:63–76
- Saji NH, Yamagata T (2003) Possible impacts of Indian Ocean Dipole mode events on global climate. *Clim Res* 25:151–169
- Saji NH, Goswami BN, Vinayachandran PN, Yamagata T (1999) A dipole mode in the tropical Indian Ocean. *Nature* 401:360–363
- Schubert SD, Park C-K (1991) Low-frequency intraseasonal tropical-extratropical interactions. *J Atmos Sci* 48:629–650
- Silvestri GE, Vera CS (2003) Antarctic Oscillation signal on precipitation anomalies over southeastern South America. *Geophys Res Lett* 30:2115. doi:10.1029/2003GL018277
- Smith TM, Reynolds RW, Peterson TC, Lawrimore J (2008) Improvements to NOAA's historical merged land–ocean surface temperature analysis (1880–2006). *J Clim* 21:2283–2296
- Terry P, Delecluse P, Labattu S, Terry L (2003) Sea surface temperature associations with the late Indian summer monsoon. *Clim Dynam* 21:593–618
- Thompson DWJ, Wallace JM (2000) Annular modes in the extratropical circulation. part I: month-to-month variability. *J Clim* 13:1000–1016
- Ting M, Hoerling MP, Xu T, Kumar A (1996) Northern Hemisphere teleconnection patterns during extreme phases of the zonal-mean circulation. *J Clim* 9:2614–2640

- Trenberth KE, Stepaniak DP (2001) Indices of El Niño evolution. *J Clim* 14:1697–1701
- Vera C, Silvestri G, Barros V, Carril A (2004) Differences in El Niño response over the Southern Hemisphere. *J Clim* 17:1741–1753
- von Storch H, Zwiers FW (1999) *Statistical analysis in climate research*. Cambridge University Press, p 484
- Walker GT, Bliss EW (1932) World weather V. *Mem R Meteor Soc* 4:53–84
- Wang H, Ting M (2000) Covariabilities of winter U.S. precipitation and Pacific sea surface temperatures. *J Clim* 13:3711–3719
- Weng H, Ashok K, Behera S, Rao SA, Yamagata T (2007) Impacts of recent El Niño Modoki on dry/wet conditions in the Pacific rim during boreal summer. *Clim Dyn* 29. doi:[10.1007/s00382-008-0394-6](https://doi.org/10.1007/s00382-008-0394-6)
- Wilks DS (2006) *Statistical methods in the atmospheric sciences*, 2nd edn. Elsevier, Amsterdam, p 627